ARMY RESEARCH LABORATORY

II. Quantitative Analysis of NO-NO_2 Mixtures by Laser Photofragmentation/Fragment Ionization at 226 and 452 nm

by Rosario C. Sausa and Robert L. Pastel

ARL-TR-2497 May 2001

The findings in this report are not to be construed as an official Department of the Army position unless so designated by other authorized documents.

Citation of manufacturer's or trade names does not constitute an official endorsement or approval of the use thereof.

Destroy this report when it is no longer needed. Do not return it to the originator.

Army Research Laboratory
Aberdeen Proving Ground, MD 21005-5066

ARL-TR-2497 **May 2001**

II. Quantitative Analysis of NO-NO_2 Mixtures by Laser Photofragmentation/Fragment Ionization at 226 and 452 nm

Rosario C. Sausa
Weapons and Materials Research Directorate, ARL

Robert L. Pastel
Michigan Technical University

Abstract

Laser-induced photofragmentation with fragment ionization is used to detect and spectrally differentiate trace concentrations of NO_2 from NO in NO-NO_2 mixtures. A laser operating near 226 or 452 nm ionizes the target molecules, and the resulting electrons are collected with miniature electrodes. NO is detected by (1+1) resonance-enhanced multiphoton ionization by means of its $A^2\Sigma^+ \leftarrow X^2\Pi$ (0,0) transitions near 226 nm, whereas NO_2 is detected near 226 nm by laser photofragmentation with subsequent NO fragment ionization by means of both its $A^2\Sigma^+ \leftarrow X^2\Pi$ (0,0) and (1,1) transitions. The NO fragment generated from the photolysis of NO_2 is produced rovibrationally excited with a significant population in the first vibrational level of the ground electronic state ($X^2\Pi$, $v'' = 1$). In contrast, "ambient" NO has a room-temperature, Boltzmann population distribution favoring the lowest ground vibrational level ($X^2\Pi$, $v'' = 0$). Thus, discrimination is possible when the internal energy distributions of both fragment NO and ambient NO are probed. This approach is also demonstrated using visible radiation, further simplifying the experimental apparatus because frequency doubling of the laser radiation is not required. Up to three decades of NO-NO_2 mixtures are measured with limits of detection (S/N = 3) in the low ppb for both NO and NO_2 for a 10-s integration time using both ultraviolet or visible radiation.

Acknowledgments

We thank Dr. A. Kotlar of the U.S. Army Research Laboratory (ARL) for may helpful discussions and gratefully acknowledge support from the American Society of Engineers (ASE) Postdoctoral Research Program.

INTENTIONALLY LEFT BLANK.

Contents

Acknowledgments iii

List of Figures vii

List of Tables ix

1. Introduction 1

2. Experimental 2

3. Results/Discussion 3

3.1 Spectral Analysis 3

3.2 Quantitative Analysis 8

4. Conclusion 14

5. References 17

Distribution List 21

Report Documentation Page 23

INTENTIONALLY LEFT BLANK.

List of Figures

Figure 1. An energy level diagram showing the PF/PI of NO_2 and REMPI of NO at 226 and 452 nm. 4

Figure 2. (a) PF/PI spectrum of NO_2 and (b) (1+1) REMPI spectrum of NO in the region of 223–227 nm. 6

Figure 3. Observed (--) and fitted (-) spectra of fragment NO generated from the UV photolysis of NO_2 (top) and ambient NO (bottom). 7

Figure 4. (a) PF/PI spectrum of NO_2 and (b) (2+2) REMPI spectrum of NO in the region of 449–455 nm. 9

Figure 5. Response plots of NO_2 at 224.4 (◆) and 226.3 nm (◊), and NO at 226.3 nm (●). 10

Figure 6. Response plots of NO_2 at 449.1 (◆) and 450.5 nm (◊), and NO at 449.1 (●) and 450.5 nm (○). 10

Figure 7. Observed (○, ●, ▽) and predicted (-) $S_{226.3\ nm}/S_{224.4\ nm}$ ratios for various NO-NO_2 mixture concentrations. The absolute NO concentrations vary from 0.06 to 21 ppm, and are slightly different for each mixture. The limiting concentrations are fixed by the NO_2 LOD, which requires a higher absolute NO concentration at larger [NO-NO_2] mixture ratios. 13

Figure 8. Observed (■, ◇, △) and predicted (-) $S_{450.5\ nm}/S_{449.1\ nm}$ ratios for various NO-NO_2 mixture concentrations. The absolute NO concentrations vary from 0.05 to 45 ppm, and are slightly different for each mixture. The limiting concentrations are fixed by the NO_2 LOD, which requires a higher absolute NO concentration at larger [NO-NO_2] mixture ratios. 14

INTENTIONALLY LEFT BLANK.

List of Tables

Table 1. REMPI and PF/PI responses (mv/ppm) of NO and NO_2, respectively. 11

Table 2. Limits of detection (ppb) of NO and NO_2 12

INTENTIONALLY LEFT BLANK.

1. Introduction

In recent years there has been much interest in the laser-based, analytical detection of NO and NO_2, referred to jointly as NOx [1, 2]. Part of this reason stems from the fact that these species are pollutants and are hazardous to the environment and to the health of the general population. They play key roles in the catalytic destruction of the ozone layer, and in the formation of acid rain and photochemical smog [3–6]. Other interest in NO and NO_2 stems from the analysis of pollutants in combustion environments [7] and the recent development of laser-based techniques for detecting energetic materials by laser photofragmenation/fragment detection (PF/FD) because these molecules are typical photolysis products of many propellants and explosives [8–12].

Conventional techniques for detecting NO and NO_2 include both chemiluminescence [13, 14] and passive collection with subsequent wet chemical analysis [15]. These methods are, however, slow and their selectivity is often insufficient to prevent interference effects at low concentrations. In order to circumvent these problems, several laser-based techniques have been employed. These include laser absorption [3–5], laser ionization [16–20], and laser photofragmentation (PF) with fragment laser-induced fluorescence (PF/LIF) [1, 2, 21, 22] or photoionization (PF/PI) [1, 2, 6, 23, 24], to name a few. In the latter technique, a laser photofragments NO_2 to NO and subsequently induces fluorescence or resonance-enhanced ionization (REMPI) of the NO fragment. These techniques are sensitive, selective, and offer real-time monitoring capabilities.

The analytical application of laser ionization for NO and NO_2 ambient detection has been studied with ultraviolet or visible laser radiation with time-of-flight mass spectrometers or miniature electrodes. Mass spectrometers have the advantage of mass selectivity over miniature electrodes, but they are bulkier and cannot be incorporated in small devices such as hand held sensors or the tip of cone penetrometers, as can miniature electrodes. NOx is spectrally differentiated from atmospheric species such O_2 and N_2 solely on excitation wavelength using miniature electrodes. Several schemes employed for NO detection using miniature electrodes include (1+1) REMPI near 226 nm using its $A^2\Sigma^+ \leftarrow X^2\Pi$ (0,0) band, (2+1) REMPI near 384 nm using its $C^2\Pi \leftarrow X^2\Pi$ (0,0) band, and (2+2) REMPI near 452 nm using its $A^2\Sigma^+ \leftarrow X^2\Pi$ (0,0) band [1, 2]. NO_2 is photolyzed efficiently at these wavelengths, and the resulting NO fragment can also be detected by the above-mentioned REMPI approaches. Typical limits of detection range from low parts-per-billion (ppb) for NO to tens of ppb for NO_2.

Although high sensitivities have been demonstrated for NOx detection by PF/PI using miniature electrodes, discrimination between NO and NO_2 is not possible

because only the total NO^+ signal, representing the sum of ambient NO and NO from NO_2, is measured. The ability to differentiate between NO and NO_2 is often desirable because of their difference in toxicity levels. The U.S. Federal Environmental Protection Agency has established a National Ambient Air Quality Standard threshold limit of 25 parts-per-million (ppm) for NO with concentrated exposures not to exceed 100 ppm for 15 min [25]. NO_2, on the other hand, is estimated to be 30 times more toxic than NO [25].

Recently we reported on the detection of NO_2 in the presence of NO by PF/PI using visible laser radiation [26]. In this report, we present our results on the trace detection, spectroscopic differentiation, and quantitative analysis of NO and NO_2 in NO-NO_2 mixtures using ultraviolet laser radiation near 226 nm. NO is detected by (1+1) REMPI using its $A^2\Sigma^+ \leftarrow X^2\Pi$ (0,0) transitions, whereas NO_2 is detected by monitoring its NO photofragment by (1+1) REMPI using its $A^2\Sigma^+ \leftarrow X^2\Pi$ (1,1) transitions. The two species are differentiated by probing the internal rovibrational distributions of both ambient and fragment NO. The analytical merit of this technique is demonstrated by measuring three decades of NO-NO_2 mixtures and determining the limits of detection at several ultraviolet wavelengths. This technique is also demonstrated using visible laser radiation, and the amounts of NO and NO_2 in various NO-NO_2 mixtures are quantified. The results are presented and compared to those obtained by other laser-based techniques.

2. Experimental

The experimental apparatus used for the present study has been reported previously [26]. Briefly, an excimer-pumped dye laser (Lumonics, HYPER EX-400 and HYPER DYE-300) operating at 10 Hz provides tunable visible radiation between 444 and 456 nm (coumarin 450). The laser line width is 0.07 cm^{-1}, and the pulse energy is approximately 10 mJ. A second-harmonic generator (HYPER TRACK-1000) that is added to the dye laser generates ultraviolet radiation between 222 and 228 nm. The UV laser linewidth is approximately twice that of the fundamental, and the pulse energy is about 100 μJ. A joulemeter (Molectron Detector, J4-05) monitors the laser energy between measurements and during the spectral scans. The laser is directed by two prisms (Suprasil) and focused by a 120-mm lens (Suprasil) into the sample cell housing a pair of ~ 1.5-cm^2 electrodes with a 0.3-cm gap. The miniature electrodes are constructed in our laboratory with stainless steel and biased at a 400-V difference for all measurements.

The sample cell is a six-arm stainless steel cross; each arm is 4 cm in diameter with a volume of about 350 cm^3. CaF_2 windows mounted on apposing arms provide optical access to the cell, and a flange, which is fitted with a vacuum connector, provides mounting and electrical feed-through for the electrodes. A mechanical

pump draws the sample gas through the cell, and a needle valve, located up-stream of the cell, regulates the flow rate (~500 cm^3/min). Flowing the samples at this rate for an effective laser probe volume of ~10^{-5} cm^3, using a pathlength of 2 mm and a focal area of $6x10^{-5}$ cm^2, prevents the built-up of the photolysis products. The sample gas pressure is monitored with a capacitance manometer (Edwards 600A-1000T-R16-H21X) and is maintained at 100 Torr for all experiments.

The bottled gases are 0.1% NO in N_2 (Union Carbide), 500 ppm NO_2 in N_2 (Matheson, <99.999%), and N_2 (Matheson, <99.999%). Various NO and NO_2 concentrations and different NO-NO_2 mixtures are prepared by serial dilution with N_2. A relatively high initial NO_2-N_2 cylinder concentration minimizes any inaccuracies in the NO_2 concentration because of potential NO_2 degradation in the cylinder. Fried et al. [27, 28] showed that the NO_2-air concentration (2.3–2500 ppm) of a number of cylinders from different vendors was actually lower than that which was reported. As much as a 60% difference was observed for NO_2-air cylinders containing NO_2 concentrations of less than 10 ppm, compared to a difference of ~5% for 500 ppm NO_2-air cylinders [27].

The ion signal from the electrodes is amplified by a current amplifier (Keithly 427, gain 10^5-10^6 V/A, time constant 0.01 ms) and displayed on a 125-MHZ oscilloscope (LeCroy 9400). The responses are 100-shot averages of the signal's peak voltage, read directly off the oscilloscope. Ionization spectra are recorded by sampling the amplified ion signal with a boxcar (Stanford Research Systems SR250) which is interfaced to a personal computer. The background noise is the standard deviation of 20 measurements, each recorded with the laser operating at the photoionization frequencies and only N_2 flowing through the sample cell. The limiting noise in this study is due mostly to fluctuations in the background ionization.

3. Results/Discussion

3.1 Spectral Analysis

The photophysical processes underlying our approach can be understood by referring to the potential energy level diagrams in Figure 1 which show the REMPI of NO and PF/PI of NO_2. The NO molecule is suitable for UV REMPI detection because it has a relatively large absorption cross section at 226 nm [5], ~6.6×10^{-18} cm^2, and the ionization proceeds through a real, intermediate state ($A^2\Sigma^+$, $\tau \sim$ 215 ns), which enhances the ionization because its energy is resonant with the energy of one 226-nm photon. The overall effect is a large ionization cross section of ~7×10^{-19} cm^2 at 226 nm [29]. The Boltzmann population distribution of NO favors the v″= 0 level of its ground electronic state at room temperature, and the ionization is thus accomplished by means of its $A^2\Sigma^+ \leftarrow X^2\Pi$ (0,0) transitions. The visible

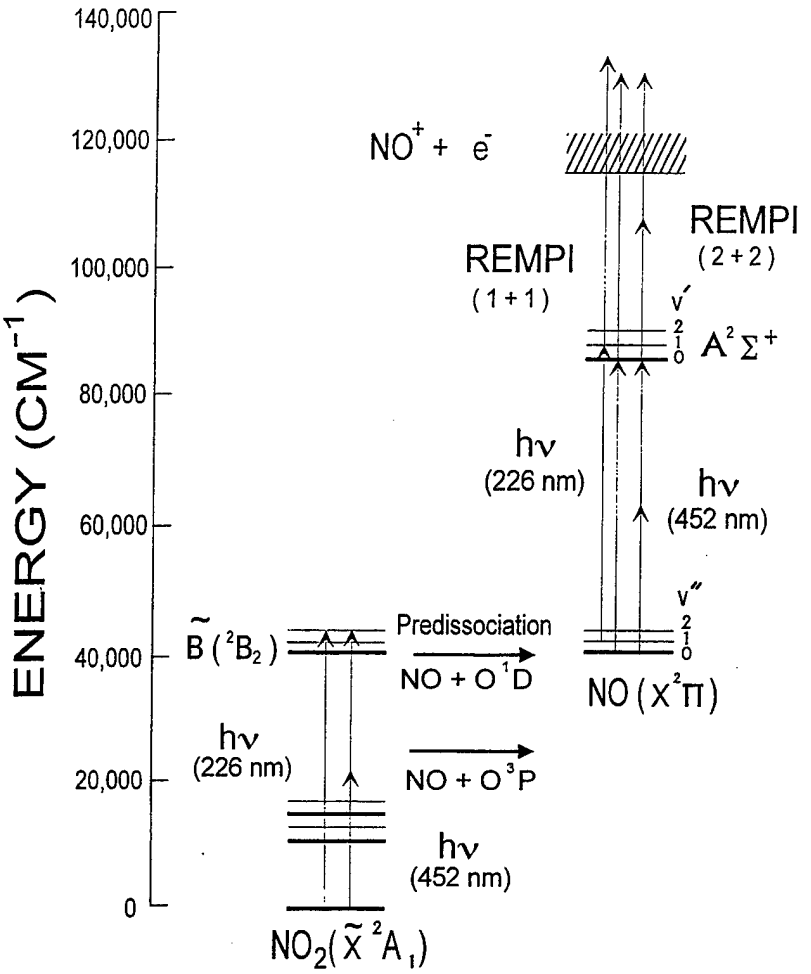

Figure 1. An energy level diagram showing the PF/PI of NO_2 and REMPI of NO at 226 and 452 nm.

ionization of NO is a four-photon process proceeding through the two-photon resonant $A^2\Sigma^+$ intermediate state.

The NO_2 PF/PI process is also depicted in Figure 1. Between 224 and 227 nm, a single photon excites NO_2 to its $\tilde{B}\,^2B_2$ state, where it subsequently predissociates into NO ($X^2\Pi$) + O (^3P) and NO ($X^2\Pi$) + O (^1D) with lifetimes less than 40 ps [30, 31]. The resulting NO fragment, which is formed rovibrationally excited with a significant fraction in the $v'' = 1$ level of the ground electronic state, is then ionized by a (1+1) REMPI process by means of its NO $A^2\Sigma^+ \leftarrow X^2\Pi$ (1,1) transitions. Spectral differentiation between NO and NO_2 is thus possible by probing the internal population distributions of both ambient and fragment NO. When visible radiation is used for the NO_2 PF/PI process, it is similar to the process when uv radiation is used but requires double the photons for both photofragmentation and ionization processes. Morrison et al. [32] studied the photofragmentation dynamics of NO_2 over the range of 420-520 nm in both collisional (few Torr) and collision-free

(10^{-5} Torr) environments. The dynamics of these processes were determined to depend on both wavelength and pressure. Morrison et al. [32] report that in a collision-free environment at wavelengths ranging from 475–490 nm, NO_2 dissociates into NO ($X^2\Pi$) + O (^3P), whereas at wavelengths less than 475 nm it dissociates into NO ($X^2\Pi$) + O (^1D). In a collisional environment the O (^3P) channel is favored down to 420 nm [32]. The collision-free photodissociation of NO_2 at 450 nm produces NO in its $X^2\Pi$ (v″=0) and (v″=1) levels compared to that at 226 nm, which produces NO vibrationally inverted in the v = 2 level [30].

Figure 2 shows UV excitation spectra of ~100 ppm of NO and 500 ppm of NO_2 at 298 K and 100 Torr in the region of 223.5–227 nm. The spectra are not corrected for laser energy, which diminishes in the low wavelength region due to the tuning limit of the second-harmonic crystal. The ambient NO spectral features arise from $A^2\Sigma^+ \leftarrow X^2\Pi$ (0,0) transitions in the 223–227 nm region, whereas those from fragment NO arise from both NO $A^2\Sigma^+ \leftarrow X^2\Pi$ (1,1) transitions in the 223–224 nm region and (0,0) transitions. The P_1, Q_1, P_{21}, P_2, and Q_{12} branch heads in the (0,0) band are labeled for both ambient and fragment NO. Figure 2 reveals that the spectral features of both ambient NO and fragment NO are rotationally resolved at 100 Torr, and that a significant amount of fragment NO is formed vibrationally excited in its ground electronic state ($X^2\Pi$). A comparison of the spectral features in the (1,1) band to those in the (0,0) band reveals that they are about equal, if one accounts for the variation in laser energy in the two band regions. In contrast, Bigio et al. [30] measure a (1,1)/(0,0) band ratio of ~0.4 using the Q_1 rotational lines for the 226-nm photolysis of free-jet NO_2 in a high vacuum apparatus equipped with a quadrupole mass spectrometer. Through band contour analysis, they determined the NO (v″ = 1/v″ = 0) vibrational branching ratio to be ~ 0.6. Our results probably differ from those of Bigio et al. because of the different experimental pressures used (100 Torr vs. ~10^{-5} Torr) resulting in different photodissociation dynamics. Vibrational relaxation is negligible in the timescales of both experiments.

Figure 3 shows the observed and calculated excitation spectra of fragment NO generated from NO_2 and room temperature NO in the region of 226.3–226.8 nm. The laser energy is fairly constant throughout this region. The calculated spectrum is fitted to the observed spectrum using a multiparameter computer program based on a Boltzmann rotational distribution analysis [33]. The parameters include the laser line shape, temperature, and absolute and relative frequency values for the data and total NO population. The program utilizes one-photon line strengths and rotational energy levels calculated using ground and excited electronic spectroscopic constants for NO reported by Henry et al. [34] and Engleman and Rouse [35] respectively, and a radiative lifetime reported by McDermid and Laudenslager [36]. The line strengths associated with the nonresonant, continuum transitions from the $A^2\Sigma^+$ state are assumed to be equal [37]. To test the program and verify our assumption, we fitted a REMPI spectrum of room temperature NO using a Lorentzian function for the line shape. The observed and fitted spectrum

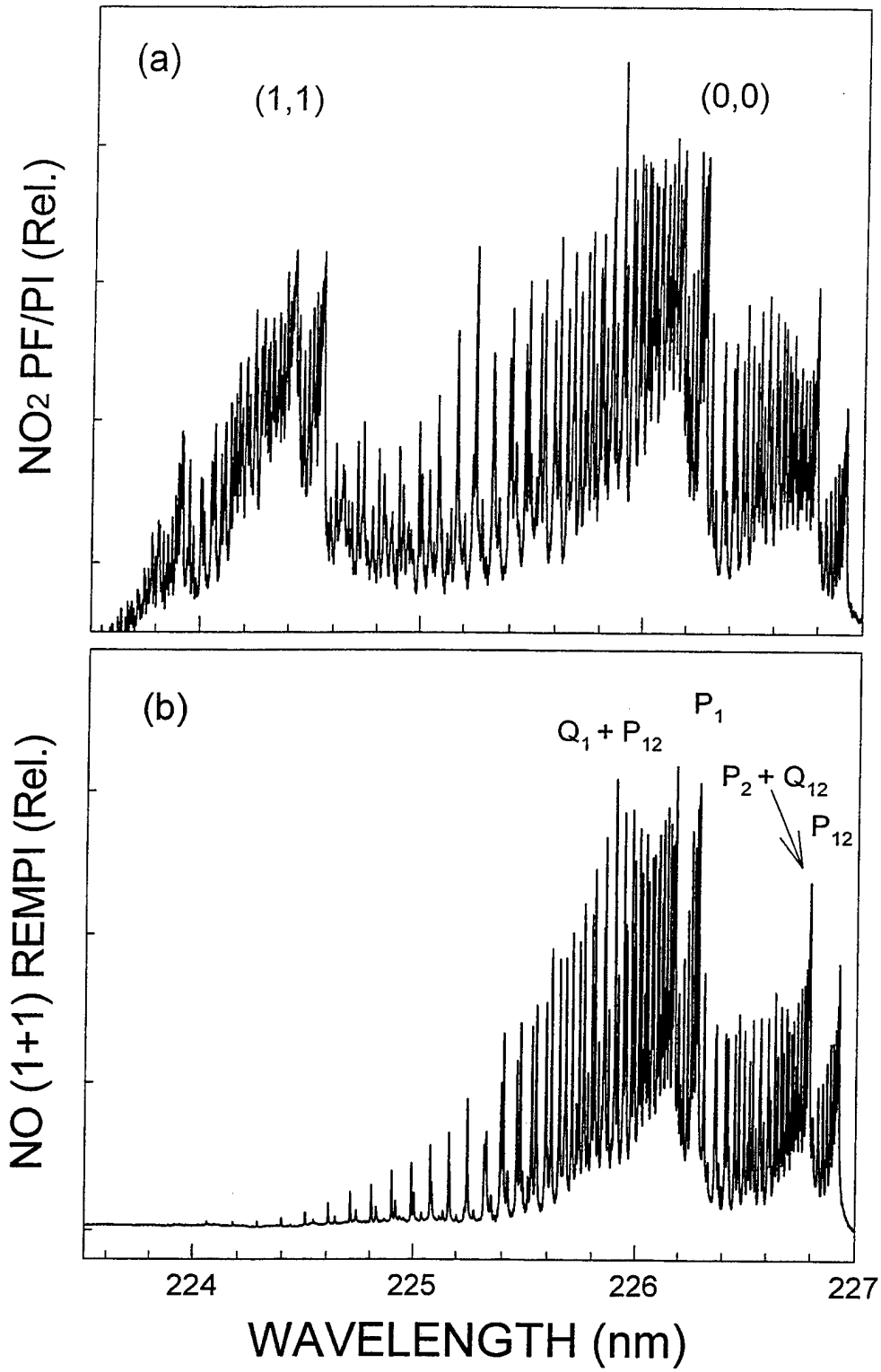

Figure 2. (a) PF/PI spectrum of NO_2 and (b) (1+1) REMPI spectrum of NO in the region of 223-227 nm.

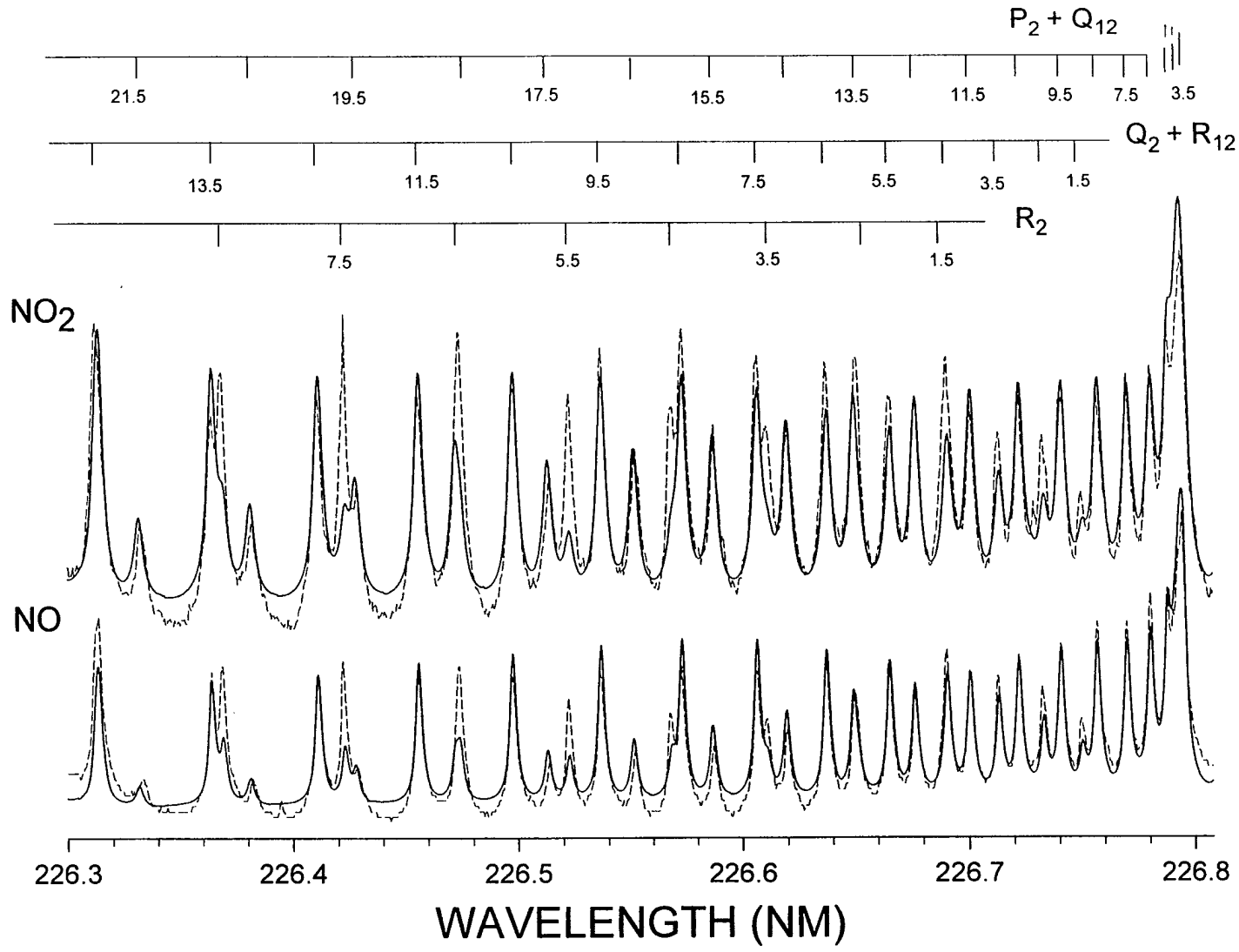

Figure 3. Observed (--) and fitted (-) spectra of fragment NO generated from the UV photolysis of NO_2 (top) and ambient NO (bottom).

are shown in the bottom of Figure 3. Overall, the calculated spectrum fits the observed data rather well, particularly for the P_2, Q_{12}, Q_2, and R_{12} rotational levels. The observed and calculated R_2 rotational levels do not agree as well as the other rotational levels. The best fit of the observed data yields a rotational temperature of 350 ± 50 K. Rotational analysis of fragment NO generated from the photolysis of NO_2 yields a temperature of 600 ± 100 K, suggesting that thermal equilibration has not been established at 100 Torr. Similar results are obtained from the rotational analysis of the NO $A^2\Sigma^+ \leftarrow X^2\Pi$ (1,1) branches. For comparison, Bigio et al. [30] determined a $T_{rot} \sim 1600$ K for both the (0,0) and (1,1) bands in the collisionless dissociation of NO_2 at 227 nm through band contour analysis. Our results are consistent with those of Bigio et al. because collisions help thermalize the nascent NO distribution, thus lowering the temperature. For our experimental conditions, NO_2 experiences ~ 10 collisions with the buffer gas within the laser pulse duration.

Figure 4 shows visible excitation spectra of ~128 ppm of NO and 500 ppm of NO_2 at 298 K and 100 Torr in the region of 448.5–455 nm. The laser energy is relatively constant throughout this spectral region, and the shot-to-shot laser energy variation is about 10%. The NO_2 spectral features correspond mostly to NO $A^2\Sigma^+ \leftarrow X^2\Pi$ (0,0) and (1,1) rotational lines resulting from the two-photon dissociation of NO_2 to NO followed by (2+2) ionization of the NO fragment, whereas those of ambient NO correspond mostly to NO $A^2\Sigma^+ \leftarrow X^2\Pi$ (0,0) rotational lines resulting from the (2+2) REMPI of NO. The prominent features of both spectra result from two-photon selection rules governing the (2+2) REMPI process by means of the resonant $A^2\Sigma^+$ state. Thus, the visible REMPI spectra exhibit strong main O and S branches ($\Delta J = \pm 2$), in addition to the P, Q, and R branches ($\Delta J = 0, \pm 1$) observed in the UV (1+1) REMPI spectra. The NO_2 spectral feature near 449.1 nm, resulting from the photodissociation of NO_2 to NO and subsequent ionization of NO $X^2\Pi$ ($v''=1$), indicates that NO is formed vibrationally excited. This feature is not observed in the ambient NO spectrum and is thus used for monitoring NO_2 in the presence of NO. The intensity of this feature is about twice that of its analogous (0,0) feature near 453.8 nm. A comparison between the (1,1) and (0,0) spectral features in the visible to those in the UV reveals that the efficiency of NO $X^2\Pi$ ($v''=1$) formation is about a factor of two greater when NO_2 is photolyzed with visible wavelengths compared to UV wavelengths. The rotational lines in the O_{12} branch, two of which are labeled b and c in Figure 4 and the one labeled "a" near 450.5 nm, are unusually strong and result from a double resonance process where both the second and third photon are resonant with excited states of NO. The overall process is therefore described as a (2+1+1) REMPI process [38, 39]. Rotational analysis of the $O_{22} + P_{12}$ branch near 453.8 nm yields rotational temperatures of 290 ± 10 K for ambient NO and 500 ± 100 K fragment NO [26].

3.2 Quantitative Analysis

Figure 5 shows the response curves for NO_2 at 224.4 and 226.3 nm and for NO at 226.3 nm. Figure 6 shows the response curves for NO_2 at 449.1 and 450.5, and

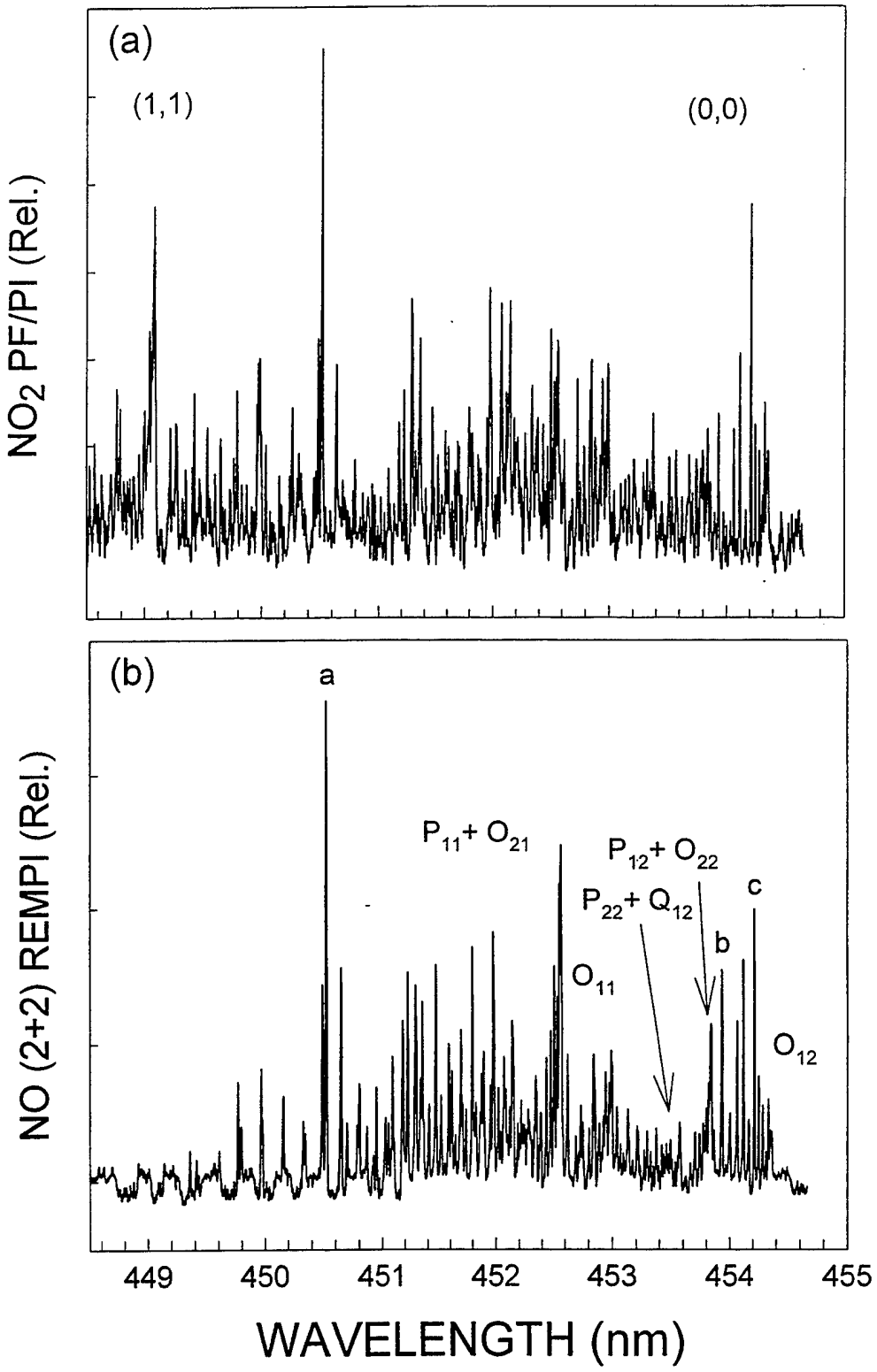

Figure 4. (a) PF/PI spectrum of NO_2 and (b) (2+2) REMPI spectrum of NO in the region of 449–455 nm.

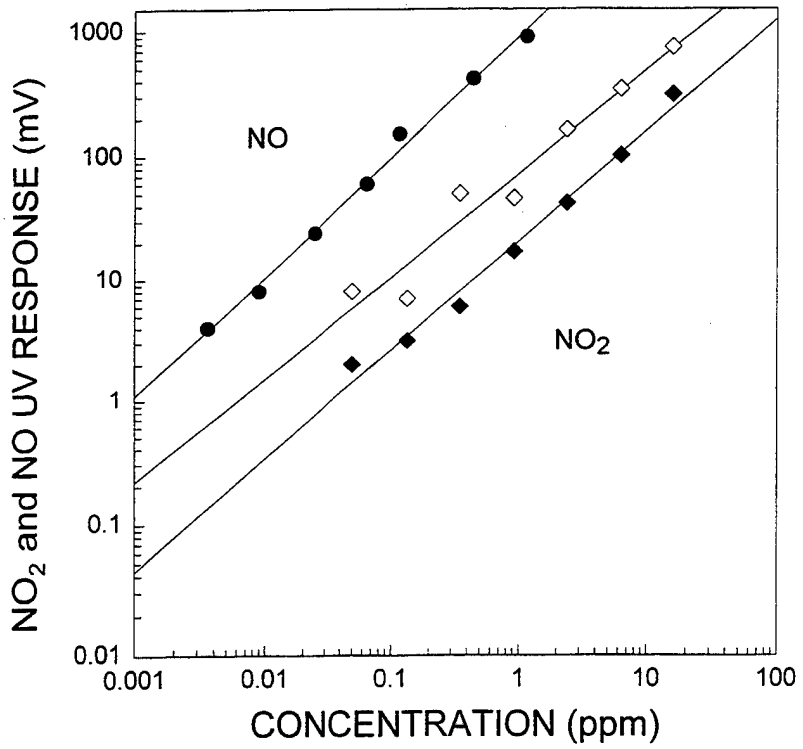

Figure 5. Response plots of NO_2 at 224.4 (◆) and 226.3 nm (◊), and NO at 226.3 nm (●).

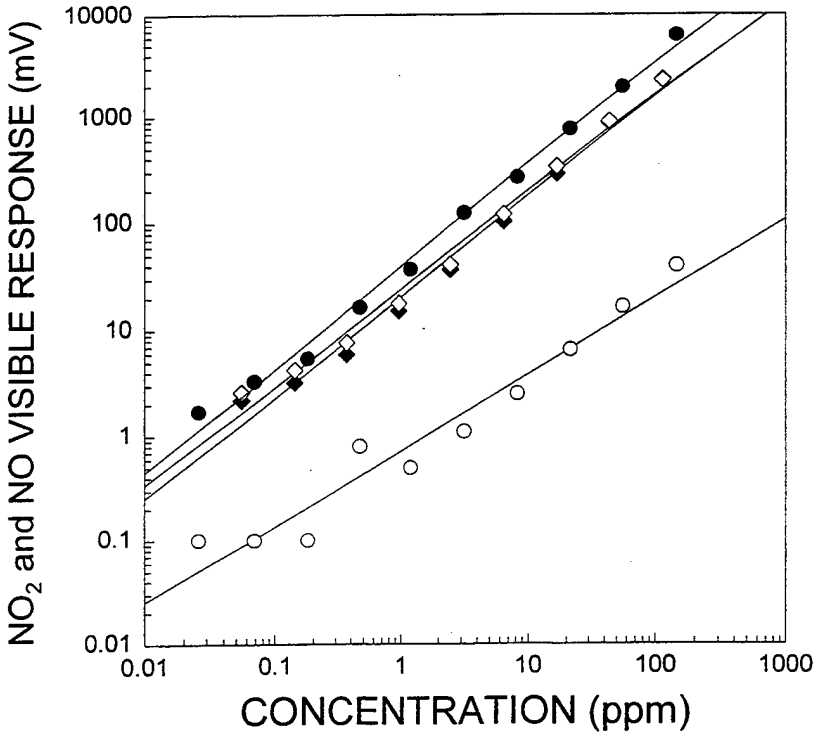

Figure 6. Response plots of NO_2 at 449.1 (◆) and 450.5 nm (◊), and NO at 449.1 (●) and 450.5 nm (○).

NO at 449.1 and 450.5 nm. In both Figures 5 and 6, the solid straight lines are best fits to the data, which are represented by symbols. For a fixed optical setup and laser energy, the responses are directly proportional to the NO and NO_2 concentration. The UV and visible responses are linear over three and four decades of concentrations, respectively, and their slopes are listed in Table 1. The large response of NO at 226.3 nm compared to 224.4 nm is due to the large NO population of the $X^2\Pi$ v = 0 level compared to at $X^2\Pi$ v = 1 level at room temperature. The NO_2 PF/PI responses at 226.3 and 224.4 nm are within a factor of two of each other and indicate that NO is formed vibrationally excited in the photolysis of NO_2. Table 1 also shows that the response of NO at 450.9 nm is about twice that at 454.4 nm. This is attributed to an enhancement resulting from double resonance processes. The response of NO at 449.1 nm is the smallest and results from an unfavorable Boltzmann population of the $X^2\Pi$ (v = 1) level at room temperature. The NO_2 response at 449.1 nm, which is nearly the same as that at 450.5 nm, is twice that at 454.4 nm, suggesting that the photodissociation of NO_2 with visible laser radiation favors the formation of NO $X^2\Pi$ (v = 1) over NO $X^2\Pi$ (v = 0).

Table 1. REMPI and PF/PI responses (mv/ppm) of NO and NO_2, respectively.

Compound	Wavelength				
	224.4 nm	226.3 nm	449.1 nm	450.5 nm	454.4 nm
NO	4.5	779.0	0.273	41.82	22.58
NO_2	19.25	46.0	20.01	19.85	10.6

The limits of detection (LOD) of NO and NO_2 at several UV and visible wavelengths are listed in Table 2. The LOD is defined by $3\sigma/R$, where R is the response and σ is the root mean square (rms) of the noise. The rms of the noise is the measured standard deviation of 20 independent measurements, each a 100-shot average of the signal recorded without sample with N_2 flowing through the sample cell and with the laser operating at the photoionization wavelength. Table 2 reveals that the LODs of NO and NO_2 are respectively 2.5 ppm and 29 ppb at 224.4 nm, and 2 and 32 ppb at 226.3 nm. The 226.3-nm values are similar to those previously determined in our laboratory [24]. The high sensitivities achieved by PF/PI using ultraviolet radiation are a reflection of the high efficiencies of both photofragmentation and ionization processes employed. As expected, NO_2 has a lower sensitivity than NO at 226.3 nm because of the following reasons: (1) NO_2 may not be 100% photolyzed when excited with 226.3-nm radiation; (2) less laser energy is available for NO fragment ionization because a portion of it is expended for NO_2 fragmentation; and (3) the laser radiation is resonant only with a fraction of the NO molecules generated because the NO fragment is formed in a wide distribution of rovibrational levels; or a combination of all three is possible. The LODs of NO are 5 and 9 ppb at 450.5 and

Table 2. Limits of detection (ppb) of NO and NO_2.

Compound	Wavelength				
	224.4 nm	226.3 nm	449.1 nm	450.5 nm	454.4 nm
NO	2500	2	769	5	9
NO_2	29	32	10.5	10.5	19

454.4 nm, respectively, both larger than the LOD of NO at 226.2 nm (2 ppb). The lower sensitivity with visible wavelengths is attributed to a lower NO ionization efficiency when using visible radiation compared to ultraviolet radiation. The higher sensitivity of NO and NO_2 at 450.5 nm compared to 454.4 nm is attributed mainly to a higher ionization efficiency at 450.5 nm because of double resonance processes occurring during ionization. Table 2 also reveals that the visible NO_2 LODs range from 10.5–19 ppb and compare favorably to the UV NO_2 LODs, which range from 29–32 ppb. This is in part because of the lower noise levels in the visible compared to the ultraviolet, even despite the use of much higher energies in the visible. The reduction in sensitivity that occurs in the visible because of a lower multiphoton absorption cross sections is thus offset by a corresponding reduction in background noise. The relative higher background noise in the UV results predominantly from the higher cross sections for nonresonant multiphoton ionization, which are more favorable for the two-photon process occurring in the UV than the four-photon process occurring in the visible. Thus, it is possible to use higher laser intensities in the visible without generating the same level of background.

The spectral differentiation between NO and NO_2 in NO-NO_2 mixtures can be determined by comparing the ionization responses of the two species at two different wavelengths. One wavelength, λ_0, must correspond to a rotational line of the NO $A^2\Sigma^+ \leftarrow X^2\Pi$ (0,0) band, whereas the other wavelength, λ_1, must correspond to a rotational line of the NO $A^2\Sigma^+ \leftarrow X^2\Pi$ (1,1) band. The formula for the signal ratio at a mixture $M = [NO]/[NO_2]$ is

$$\frac{S(\lambda_0)}{S(\lambda_1)} = \frac{R_{NO}(\lambda_0)\ M + R_{NO_2}(\lambda_0)}{R_{NO}(\lambda_1)\ M + R_{NO_2}(\lambda_1)}, \qquad (1)$$

where $R_{NO}(\lambda)$ and $R_{NO_2}(\lambda)$ are the NO and NO_2 ionization responses, respectively, at the selected wavelengths. The signal ratio is dependent on the mixture $M = [NO]/[NO_2]$, and not on the absolute concentration of NO or NO_2. Equation (1) is verified by observing the total ionization response at the two photoionization wavelengths selected for many NO-NO_2 mixtures. In order to verify that equation (1) is only dependent on M, the mixtures were diluted with N_2 and re-evaluated.

The NO and NO_2 differentiation experiments are performed by premixing NO and NO_2, typically at 150 ppm, and recording the REMPI signal at the photoionization wavelengths. The mixture is diluted with N_2, and the observations are repeated.

Figure 7 compares the observed data with that predicted using equation (1) and the responses at 224.4 and 226.3 nm in Table 1. The curve shown is the predicted response and not a best fit to the experimental data. The series of symbols at the same mixture represent different dilutions of the NO-NO_2 mixture. The data at the same mixture cluster together, suggesting that the ratio is dependent only on the mixture and not the absolute concentrations. All the data lie close to the curve, implying that equation (1) can be used to predict mixtures of NO and NO_2. The valid range of mixtures is determined from the linear dynamic range of the detection method for both NO and NO_2. The figure shows good agreement over two decades of mixtures.

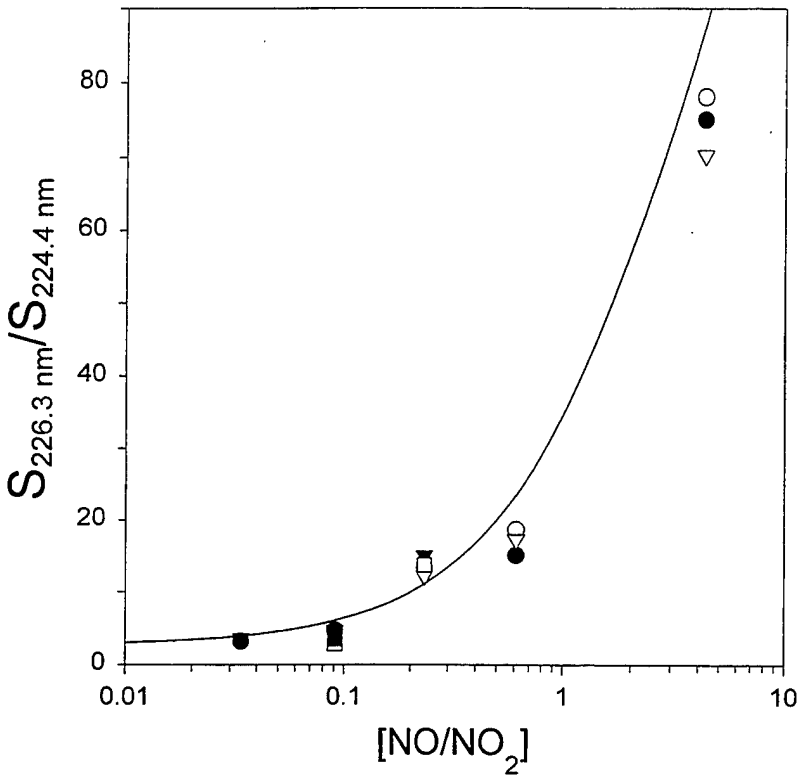

Figure 7. Observed (O, ●, ▽) and predicted (-) $S_{226.3\ nm}/S_{224.4\ nm}$ ratios for various NO-NO_2 mixture concentrations. The absolute NO concentrations vary from 0.06 to 21 ppm, and are slightly different for each mixture. The limiting concentrations are fixed by the NO_2 LOD, which requires a higher absolute NO concentration at larger [NO-NO_2] mixture ratios.

Figure 8 compares the data collected from NO-NO_2 mixtures with that predicted using equation (1) with the responses at 450.5 and 449.1 nm from Table 1. The predicted curve agrees well with the observed data for over three decades of NO-NO_2 mixtures. Visible wavelengths are approximately an order of magnitude more differentiating than UV wavelengths because the NO_2/NO response ratio at 449.5 nm is about ten times greater than that at 224.4 nm.

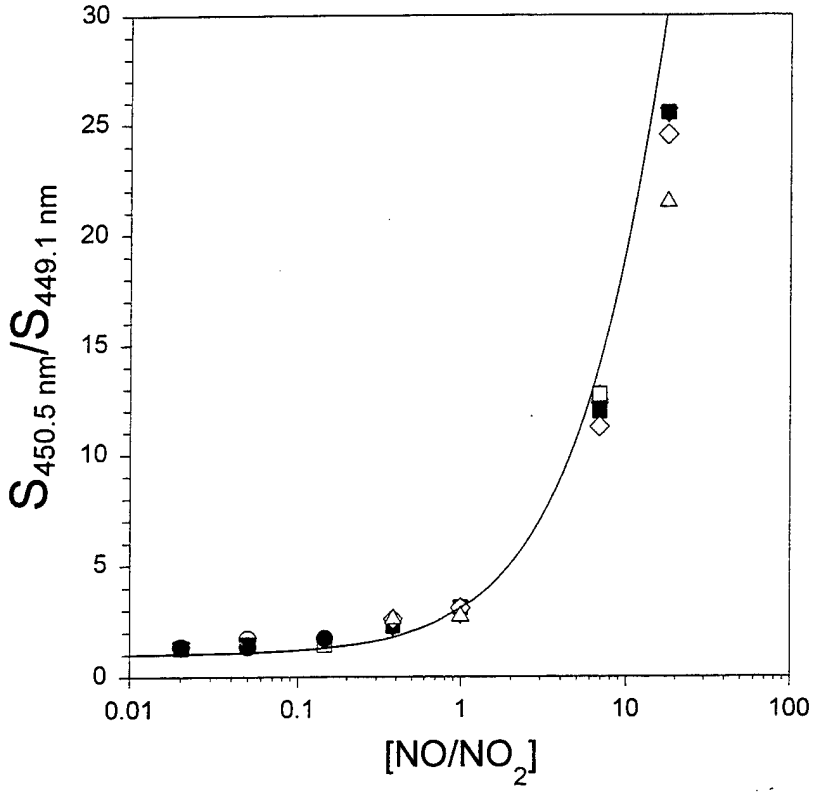

Figure 8. Observed (■, ◇, △) and predicted (-) $S_{450.5\ nm}/S_{449.1\ nm}$ ratios for various NO-NO_2 mixture concentrations. The absolute NO concentrations vary from 0.05 to 45 ppm, and are slightly different for each mixture. The limiting concentrations are fixed by the NO_2 LOD, which requires a higher absolute NO concentration at larger [NO-NO_2] mixture ratios.

4. Conclusion

A method for the detecting and spectrally differentiating between NO and NO_2 in NO-NO_2 mixtures has been demonstrated. The method is based on the REMPI detection of NO and the laser photofragmentation of NO_2 with subsequent REMPI detection of the NO photofragment using two wavelengths in the visible or UV for probing the ground and first vibrational state of ambient and fragment NO ($X^2\Pi$). Spectral differentiation of NO_2 from ambient NO is possible because the visible and UV photolysis of NO_2 results in the formation of NO in both its $X^2\Pi$ ($v'' = 1$) and ($v'' = 0$) states, whereas the Boltzmann population distribution of ambient NO favors the ($v'' = 0$) state at room temperature. The analytical utility has been demonstrated for over three decades of NO-NO_2 mixtures and many concentrations. Response curves for both NO and NO_2 have been measured and LODs determined at several UV and visible wavelengths. The LODs for NO and NO_2 are respectively 2 and 32 ppb at 226.3 nm, and 5 and 10 ppb at 450.5 nm. The lower sensitivity in the

visible is attributed to both a lower NO_2 photofragmentation efficiency and NO ionization efficiency in the visible compared to the UV.

INTENTIONALLY LEFT BLANK.

5. References

1. Simeonsson, J. B., and R. C. Sausa. "Laser Photofragmentation/Fragment Detection Techniques for Chemical Analysis of the Gas Phase." *TRAC-Trends in Analytical Chemistry*, vol. 17, nos. 8 and 9, pp. 542–550, 1998, and references therein.

2. Simeonsson, J. B., and R. C. Sausa. "A Critical Review of Laser Photofragmentation/Fragment Detection Techniques for Gas Phase Chemical Analysis." *Applied Spectroscopy Reviews*, vol. 31, pp. 1–72, 1996, and references therein.

3. Nelson, D. D., M. S. Zahniser, J. B. McManus, C. E. Kolb, and L. J. Jimenez. "A Tunable Diode Laser System for the Remote Sensing of On-Road Vehicle Emissions." *Applied Physics B- Lasers and Optics*, vol. 67, no. 4, pp. 433–441, 1998.

4. Kolsch, H. J., P. Rairoux, J. P. Wolf, and L. Woste. "Simultaneous NO and NO_2 Dial Measurement Using BBO Crystal." *Applied Optics*, vol. 28, pp. 2052–2056, 1989.

5. Alden, M., H. Edner, and S. Svanberg. "Laser Monitoring of Atmospheric NO Using Ultraviolet Differential-Absorption Techniques." *Optics Letters*, vol. 7, pp. 543–545, 1982.

6. Peng, W. X., K. W. D. Leddingham, A. Marshall, and R. P. Singhal. "Urban Air-Pollution Monitoring: Laser-Based Procedure for the Detection of NOx Gases." *Analyst*, vol. 120, pp. 2537–2542, 1995.

7. Stenberg, J., R. Hernberg, and J. Vattulainen. "Analysis of Pollutant Chemistry in Combustion by In Situ Pulsed Photoacoustic Laser Diagnostics." *Applied Optics*, vol. 34, no. 6, pp. 8400–8408, 1995.

8. Swayambunathan, V., G. Singh, and R. C. Sausa. "Laser-Photofragmentation-Fragment Detection and Laser-Pyrolysis-Laser-Induced Fluorescence Studies on Energetic Materials." *Applied Optics*, vol. 38, no. 30, pp. 6447–6454, 1999.

9. Wu, D., J. Singh, F. Yueh, and D. Monts. "2,4,6-Trinitrotoluene Detection by Laser-Photofragmentation/Laser-Induced Fluorescence." *Applied Optics*, vol. 35, no. 21, pp. 3998–4003, 1996.

10. Boudreaux, G. M., T. S. Miller, A. J. Kunefke, J. P. Singh, F. Yueh, and D. Monts. "Development of a Photofragmentation Laser-Induced-Fluorescence Laser Sensor for Detection of 2,4,6-Trinitrotoluene in Soil and Groundwater." *Applied Optics*, vol. 38, no. 6, pp. 1411–1417, 1999.

11. Lemire, G. W., J. B. Simeonsson, and R. C. Sausa. "Monitoring of Vapor-Phase Nitrocompounds Using 226-nm Radiation: Fragmentation With Subsequent NO Resonance-Enhanced Multiphoton Ionization Detection." *Analytical Chemistry*, vol. 65, pp. 529–533, 1993.

12. Marshall, A., A. Clark, K. W. D. Ledingham, J. Sander, R. P. Singal, C. Kosmidis, and R. M. Deas. "Detection and Identification of Explosives Compounds Using Laser Ionization Time-of-Flight Techniques." *Rapid Communications in Mass Spectroscopy*, vol. 8, no. 7, pp. 521–526, 1994.

13. Collins, G. E., and S. L. Rosepehrsson. "Chemiluminescence Chemical Sensors for Oxygen and Nitrogen-Dioxide." *Analytical Chemistry*, vol. 67, no. 13, pp. 2224–2230, 1995.

14. Robins, R. A., A. A. Floreani, S. G. VonEssen, J. H. Sisson, G. E. Hill, I. Rubinstein, and R. G. Townley. "Measurement of Exhaled Nitric Oxide by Three Different Techniques." *American Journal of Respiratory and Critical Care Medicine*, vol. 153, no. 5, pp. 1631–1635, 1996.

15. Glasius, M., M. F. Carlsen, T. S. Hansen, and C. Lohse. "Measurement of Nitrogen Dioxide on Funene Using Diffusion Tubes." *Atmospheric Environment*, vol. 33, pp. 1177–1185, 1999.

16. Lee, S., J. Hirokawa, Y. Kajii, and H. Akimoto. "New Method for Measuring Low NO Concentrations Using Laser Induced Two Photon Ionization." *Review of Scientific Instruments*, vol. 68, no. 7, pp. 2891–2897, 1997.

17. Benter, T., M. Liesner, V. Sauerland, and R. N. Schindler. "Mass-Spectrometric In-Situ Determination of NO_2 in Gas-Mixtures by Resonance-Enhanced Multiphoton Ionization." *Fresnius' Journal of Analytical Chemistry*, vol. 351, no. 6, pp. 489–492, 1995.

18. Kumar, G. R., and D. Mathur. "Reply to Comment on 'On the Ionization and Dissociation of NO_2 by Short, Intense Laser Pulses.'" *Chemical Physics Letters*, vol. 292, pp. 647–650, 1998, and references therein.

19. Singhal, R. P., H. S. Kilic, K. W. D. Ledingham, T. McCanny, W. X. Peng, D. J. Smith, C. Kosmidis, A. J. Langley, and P. F. Taday. "Comment on the Ionization and Dissociation of NO_2 by Short Intense Laser Pulses." *Chemical Physics Letters*, vol. 292, pp. 643–650, 1998.

20. Vijaylakahmi, K., C. P. Safvan, G. R. Kumar, and D. Mathur. "On the Ionization and Dissociation of NO_2 by Short Intense Laser Pulses." *Chemical Physics Letters*, vol. 270, no. 1–2, pp. 37–44, 1997.

21. Bradshaw, J., D. Davis, J. Crawford, G. Chen, R. Shetter, M. Muller, G. Gregory, G. Sachse, D. Blake, B. Heikes, H. Singh, J. Mastromarino, and S. Sandholm. "Photofragmentation Two-Photon Laser-Induced Fluorescence Detection of NO_2 and NO: Comparison of Measurements With Model Results Based on Airborne Observations During PEM-Tropics A." *Geochemical Research Letters*, vol. 26, no. 4, pp. 471–474, 1999.

22. Rodgers, M. O., K. A. Asai, and D. D. Davis. "Photofragmentation Laser-Induced Fluorescence: A New Method for Detecting Atmospheric Trace Gases." *Applied Optics*, vol. 19, no. 21, pp. 3597–3605, 1980.

23. Pastel R. L., and R. C. Sausa. "Detection of NO and NO_2 by (2+2) Resonance-Enhanced Multi-Photon Ionization and Photoacoustic Spectroscopy Near 454 nm." *Applied Optics*, vol. 35, no. 21, pp. 4046–4052, 1996.

24. Simeonsson, J. B., G. W. Lemire, and R. C. Sausa. "Laser-Induced Photofragmentation/Photoionization Spectrometry: A Method for Detecting Ambient Oxides of Nitrogen." *Analytical Chemistry*, vol. 66, pp. 2272–2278, 1994.

25. Last, J. A., W. M Sun, and H. Witschi. "Ozone, NO, and NO_2- Oxidant Air-Pollutants and More." *Environmental Health Perspectives*, vol. 102, Suppl. 10, pp. 179–184, 1994.

26. Simeonsson, J. B., and R. C. Sausa. "Trace Analysis of NO_2 in the Presence of NO by Laser Photofragmentation/Fragment Photoionization Spectrometry at Visible Wavelengths." *Applied Spectroscopy*, vol. 50, no. 10, pp. 1277–1282, 1996.

27. Fried, A., R. Sams, W. Dorko, J. W. Elkins, and Z. T. Cai. "Determination of Nitrogen-Dioxide in Air Compressed Gas-Mixtures by Quantitative Tunable Diode-Laser Absorption Spectrometry and Chemiluminescence Detection." *Analytical Chemistry*, vol. 60, no. 5, pp. 394–403, 1988.

28. Fried, A., L. Nunnermacker, B. Cadoff, R. Sams, N. Yates, W. Dorko, R. Dickerson, and D. E. Winstead. "Reference NO_2 Calibration System for Ground-Based Intercomparison During NASAs GTE/CITE-2 Mission." *Journal of Geophysical Research Atmospheres*, vol. 95, no. D7, pp. 10139–10146, 1990.

29. Zacharias, H., R. Schmiedl, and K. H. Welge. "State Selective Step-Wise Photoionization of NO With Mass Spectroscopic Ion Detection." *Appied Physics*, vol. 21, pp. 127–133, 1980.

30. Bigio, L., R. S. Tapper, and E. R. Grant. "The Role of Near-Resonant Intermediate States in the 2-Photon Excitation of NO_2: The Distinct Dynamics of 2-Photon Photofragmentation." *Journal of Physical Chemistry*, vol. 88, pp. 1271–1273, 1984.

31. Morrison, R. J. S., and E. R. Grant. "Dynamics of the 2-Photon Photodissociation of NO_2: A Molecular Multiphoton Ionization Study of NO Photofragment Internal Energy-Distributions." *Journal of Physical Chemistry*, vol. 77, pp. 5994–6004, 1982, and references therein.

32. Morrison, R. J. S., B. H. Rockney, and E. R. Grant. "Multiphoton Ionization of NO_2: Spectroscopy and Dynamics." *Journal of Physical Chemistry*, vol. 75, no. 6, pp. 2643–2651, 1981.

33. Vanderhoff, J. A., M. W. Teague, and A. J. Kotlar. "Detection of Temperature and NO Concentrations Through the Dark Zone of Solid-Propellant Flames." *Proceedings of the Twenty-Fourth Symposium (International) on Combustion*, pp. 1915–1922, The Combustion Institute, Pittsburgh, PA, 1992.

34. Henry, A., M. F. Le Moal, Ph. Cardinet, and A. Valentin. "Overtone Bands of $^{14}N^{16}O$ and Determination of Molecular Constants." *Journal of Molecular Spectroscopy*, vol. 70, no. 1, pp. 18–26, 1978.

35. Engleman, R., Jr., and P. E. Rouse. "The β and γ Bands of Nitric Oxide Observed During Flash Photolysis of Nitrosyl Chloride." *Journal of Molecular Spectroscopy*, vol. 37, pp. 240–251, 1971.

36. McDermid, I. S., and J. B. Laudenslager. "Radiative Lifetimes and Electronic Quenching Rate Constants for Single-Photon Excited Rotational Levels of NO ($A^2\Sigma^+$, $v'' = 0$)." *Journal of Quantitative Spectroscopy and Radiative Transfer*, vol. 27, no. 5, pp. 483–492, 1982.

37. Jacobs, D. C., R. J. Madix, and R. N. Zare. "Reduction of 1+1 Resonance-Enhanced MPI Spectra to Population-Distributions: Application to the NO ($A^2\Sigma^+ - X^2\Pi$) System." *Journal of Chemical Physics*, vol. 85, no. 10, pp. 5469–5479, 1986.

38. Miler, J. C., and R. N. Compton. "Multiphoton Ionization Studies of Ultracold Nitric-Oxide." *Journal of Chemical Physics*, vol. 84, pp. 675–683, 1986.

39. White, M. G., W. A. Chupka, M. Seaver, A. Woodward, and S. D. Colson. "Resonant Multiphoton of NO Via the $^2\Sigma^+$ State: Photoelectron-Spectra and Angular Distributions." *Journal of Chemical Physics*, vol. 80, pp. 678–686, 1984.

NO. OF COPIES	ORGANIZATION
2	DEFENSE TECHNICAL INFORMATION CENTER DTIC OCA 8725 JOHN J KINGMAN RD STE 0944 FT BELVOIR VA 22060-6218
1	HQDA DAMO FDT 400 ARMY PENTAGON WASHINGTON DC 20310-0460
1	OSD OUSD(A&T)/ODDR&E(R) DR R J TREW 3800 DEFENSE PENTAGON WASHINGTON DC 20301-3800
1	COMMANDING GENERAL US ARMY MATERIEL CMD AMCRDA TF 5001 EISENHOWER AVE ALEXANDRIA VA 22333-0001
1	INST FOR ADVNCD TCHNLGY THE UNIV OF TEXAS AT AUSTIN 3925 W BRAKER LN STE 400 AUSTIN TX 78759-5316
1	DARPA SPECIAL PROJECTS OFFICE J CARLINI 3701 N FAIRFAX DR ARLINGTON VA 22203-1714
1	US MILITARY ACADEMY MATH SCI CTR EXCELLENCE MADN MATH MAJ HUBER THAYER HALL WEST POINT NY 10996-1786
1	DIRECTOR US ARMY RESEARCH LAB AMSRL D DR D SMITH 2800 POWDER MILL RD ADELPHI MD 20783-1197

NO. OF COPIES	ORGANIZATION
1	DIRECTOR US ARMY RESEARCH LAB AMSRL CI AI R 2800 POWDER MILL RD ADELPHI MD 20783-1197
3	DIRECTOR US ARMY RESEARCH LAB AMSRL CI LL 2800 POWDER MILL RD ADELPHI MD 20783-1197
3	DIRECTOR US ARMY RESEARCH LAB AMSRL CI IS T 2800 POWDER MILL RD ADELPHI MD 20783-1197
	ABERDEEN PROVING GROUND
2	DIR USARL AMSRL CI LP (BLDG 305)

NO. OF
COPIES ORGANIZATION

ABERDEEN PROVING GROUND

15 DIR USARL
AMSRL WM BD
W R ANDERSON
S W BUNTE
C F CHABALOWSKI
R A FIFER
B E FORCH
B E HOMAN
A J KOTLAR
K L MCNESBY
M MCQUAID
M S MILLER
A W MIZIOLEK
J B MORRIS
R A PESCE-RODRIGUEZ
B M RICE
R C SAUSA

REPORT DOCUMENTATION PAGE

Form Approved
OMB No. 0704-0188

1. AGENCY USE ONLY *(Leave blank)*	2. REPORT DATE	3. REPORT TYPE AND DATES COVERED
	May 2001	Final, January 1996–June 2000

4. TITLE AND SUBTITLE

II. Quantitative Analysis of NO-NO_2 Mixtures by Laser Photofragmentation/Fragment Ionization at 226 and 452 nm

5. FUNDING NUMBERS

622618.H80

6. AUTHOR(S)

Rosario C. Sausa and Robert L. Pastel*

7. PERFORMING ORGANIZATION NAME(S) AND ADDRESS(ES)

U.S. Army Research Laboratory
ATTN: AMSRL-WM-BD
Aberdeen Proving Ground, MD 21005-5066

8. PERFORMING ORGANIZATION REPORT NUMBER

ARL-TR-2497

9. SPONSORING/MONITORING AGENCY NAMES(S) AND ADDRESS(ES)

10.SPONSORING/MONITORING AGENCY REPORT NUMBER

11. SUPPLEMENTARY NOTES

* Michigan Technical University, Dept. of Physics, Houghton, MI 49931

12a. DISTRIBUTION/AVAILABILITY STATEMENT

Approved for public release; distribution is unlimited.

12b. DISTRIBUTION CODE

13. ABSTRACT *(Maximum 200 words)*

Laser-induced photofragmentation with fragment ionization is used to detect and spectrally differentiate trace concentrations of NO_2 from NO in NO-NO_2 mixtures. A laser operating near 226 or 452 nm ionizes the target molecules, and the resulting electrons are collected with miniature electrodes. NO is detected by (1+1) resonance-enhanced multiphoton ionization by means of its $A^2\Sigma^+ \leftarrow X^2\Pi$ (0,0) transitions near 226 nm, whereas NO_2 is detected near 226 nm by laser photofragmentation with subsequent NO fragment ionization by means of both its $A^2\Sigma^+ \leftarrow X^2\Pi$ (0,0) and (1,1) transitions. The NO fragment generated from the photolysis of NO_2 is produced rovibrationally excited with a significant population in the first vibrational level of the ground electronic state ($X^2\Pi$, $v'' = 1$). In contrast, "ambient" NO has a room-temperature, Boltzmann population distribution favoring the lowest ground vibrational level ($X^2\Pi$, $v'' = 0$). Thus, discrimination is possible when the internal energy distributions of both fragment NO and ambient NO are probed. This approach is also demonstrated using visible radiation, further simplifying the experimental apparatus because frequency doubling of the laser radiation is not required. Up to three decades of NO-NO_2 mixtures are measured with limits of detection (S/N = 3) in the low ppb for both NO and NO_2 for a 10-s integration time using both ultraviolet or visible radiation.

14. SUBJECT TERMS

laser photofragmentation, NO-NO_2 analysis, fragment detection, visible laser ionization, ultraviolet laser ionization, quantitative analysis

15. NUMBER OF PAGES

28

16. PRICE CODE

17. SECURITY CLASSIFICATION OF REPORT	18. SECURITY CLASSIFICATION OF THIS PAGE	19. SECURITY CLASSIFICATION OF ABSTRACT	20. LIMITATION OF ABSTRACT
UNCLASSIFIED	UNCLASSIFIED	UNCLASSIFIED	UL

INTENTIONALLY LEFT BLANK.

USER EVALUATION SHEET/CHANGE OF ADDRESS

This Laboratory undertakes a continuing effort to improve the quality of the reports it publishes. Your comments/answers to the items/questions below will aid us in our efforts.

1. ARL Report Number/Author ARL-TR-2497 (Sausa) Date of Report May 2001

2. Date Report Received _____

3. Does this report satisfy a need? (Comment on purpose, related project, or other area of interest for which the report will be used.) _____

4. Specifically, how is the report being used? (Information source, design data, procedure, source of ideas, etc.) _____

5. Has the information in this report led to any quantitative savings as far as man-hours or dollars saved, operating costs avoided, or efficiencies achieved, etc? If so, please elaborate. _____

6. General Comments. What do you think should be changed to improve future reports? (Indicate changes to organization, technical content, format, etc.) _____

CURRENT ADDRESS

_____
Organization

_____
Name E-mail Name

_____
Street or P.O. Box No.

_____
City, State, Zip Code

7. If indicating a Change of Address or Address Correction, please provide the Current or Correct address above and the Old or Incorrect address below.

OLD ADDRESS

_____
Organization

_____
Name

_____
Street or P.O. Box No.

_____
City, State, Zip Code

(Remove this sheet, fold as indicated, tape closed, and mail.)
(DO NOT STAPLE)